# INTERNATIONAL SOCIETY FOR SOIL MECHANICS AND GEOTECHNICAL ENGINEERING

# HMC Based Inverse Analysis to Determine Position and Size of Square Cavities

Michael Conrad Koch[1], Fujisawa Kazunori[1], and Akira Murakami[1]

[1]Graduate School of Agriculture, Kyoto University, Sakyo-ku, Kyoto, Japan.
E-mail: koch.conrad.38m@st.kyoto-u.ac.jp. E-mail: fujik@kais.kyoto-u.ac.jp.

**Abstract:** The identification of cavities embedded in an elastic domain is an important inverse problem in engineering. A statistical solution that characterizes the mean and variance of the parameters of the cavity is sought. A Hamiltonian Monte Carlo (efficient variant of MCMC) based framework is employed to identify the position of a square cavity. Critical to the success of HMC is the evaluation of the gradient and the update of the parameters in such a manner that mesh distortions are eliminated. A moving mesh technique is used to update the parameters in a non-physical step, while the gradients are evaluated in a similar manner to those in the shape optimization literature. The framework is detailed and applied to the inversion of synthetic seismic data.

Keywords: Moving mesh method; shape derivatives; Hamiltonian Monte Carlo; cavity identification; inverse problem.

## 1. Introduction

Inverse problems are generally characterized by non-uniqueness and instability, i.e. many different choices of parameters may be consistent with the observed data and a small perturbation in data can cause arbitrarily large perturbation in the identified parameters. A common approach to solve these problems is to formulate the problem in least squares form along with some regularization parameter. Such an approach yields the best possible solution to the problem. In this paper, the main goal is not only to estimate the best point estimate but to obtain its complete statistical description. Markov Chain Monte Carlo (MCMC) methods are the most common kind of algorithms employed for such problems. Classical methods like Metropolis Hastings (Metropolis et al. 1953) are plagued by slow exploration rates of the parameter space owing to their random nature. A modern variant called Hamiltonian Monte Carlo (Duane et al. 1987; Neal 2011) solves this issue by enabling gradient guided motion of the parameter space in such a manner that the Hamiltonian remains constant. This reduces autocorrelation between successive samples and significantly speeds up the algorithm.

Explicit cavity estimation has been an active topic of research (Guzina and Bonnet 2004; Nguyen and Nestorović 2016). Most methods, however, lack the ability to consider a continuous variation of parameters over the parameter space which may lead to inaccurate solutions. In this paper, we propose a framework in which a continuous variation of parameters is allowed. However, this framework raises new problems, in terms of the evaluation of the gradient and the update of the parameters. The details of the framework are provided in the following sections.

## 2. Governing and Observation Equations

Consider a domain $\Omega = \{z_1, z_2\}$, where $z_1$ and $z_2$ are the Cartesian coordinates, bounded by $\Gamma$ composed of $\Gamma_g$ and $\Gamma_h$. We also consider a cavity $\Omega_c \subset \Omega$ embedded in the domain. The governing PDE for wave propagation in the domain $\Omega \setminus \Omega_c$ for $t \in [0, T]$ is given as

$$\rho \frac{\partial^2 u_i}{\partial t^2} = \frac{\partial \sigma_{ij}}{\partial z_j} + f_i \tag{1}$$

where, $\rho$ is the density, $\sigma_{ij}$, $z_j$, $u_i$ and $f_i$ represent the Cartesian components of the Cauchy stress tensor, position vector, displacement field and external force respectively. The Dirichlet boundary condition on $\Gamma_g$ is defined in the usual manner as

$$\mathbf{u} = \mathbf{g} \tag{2}$$

where $\mathbf{g}$ are some prescribed displacements specific to the problem. Lysmer-Kuhlemeyer absorbing boundary conditions (Lysmer and Kuhlemeyer 1969) are applied to $\Gamma_h$ such that

$$\sigma_n = -\rho c_p v_n \tag{3}$$
$$\tau = -\rho c_s v_s \tag{4}$$

where, $\sigma_n$ and $\tau$ are the normal and tangential component of the traction at the boundary. Similarly $v_n$ and $v_s$ are the normal and tangential velocities at the boundary node and $c_p$ and $c_s$ are the P-wave and S-wave velocity in the element at the boundary.

Let $\mathbf{u}(t)$, $\dot{\mathbf{u}}(t)$, $\ddot{\mathbf{u}}(t)$ and $\mathbf{f}(t) \in \mathbb{R}^d$ be the discretized global nodal displacement, velocity, acceleration and force vectors respectively, where $d$ are the global degrees of freedom. Suppose the discretized mesh of $\Omega \setminus \Omega_c$ contains $\tilde{d}$ nodes, then the node coordinates can be represented as $\mathbf{Z} \in \mathbb{R}^{\tilde{d} \times 2}$ where $\mathbf{Z} = (\mathbf{z}_1, \dots, \mathbf{Z}_c, \dots, \mathbf{z}_{\tilde{d}})$. Suppose a parameterization ($\boldsymbol{\theta} \in \mathbb{R}^K$) of the cavity $\Omega_c$ exists, such that the components of $\mathbf{Z}$ at the cavity boundary $\mathbf{Z}_c$ can be expressed as a function of the parameters $\boldsymbol{\theta}$ i.e. $\mathbf{Z}_c = (\mathbf{z}_{c1}(\boldsymbol{\theta}), \dots, \mathbf{z}_{c\tilde{d}}(\boldsymbol{\theta}))$ then the semi-discretized weak form of Eq. (1) is written as

$$\mathbf{M}(\boldsymbol{\theta})\ddot{\mathbf{u}}(t) + \mathbf{C}(\boldsymbol{\theta})\dot{\mathbf{u}}(t) + \mathbf{K}(\boldsymbol{\theta})\mathbf{u}(t) = \mathbf{f}(t) \tag{5}$$

The matrices $\mathbf{M}$, $\mathbf{C}$ and $\mathbf{K}$, which are parameter dependent, are the usual mass, damping and stiffness matrices respectively. Eq. (5) represents the forward equation which needs to be solved for a particular $\boldsymbol{\theta}$.

The inverse problem necessitates a measurement model. Let $\mathbf{x}_k \in \mathbb{R}^D$ be the state vector (usually a function of $\boldsymbol{\theta}$) at discrete instances in time $k \in \{1, \dots, n\}$, and observations $\mathbf{y}_k \in \mathbb{R}^m$ be corrupted by some Gaussian noise $\mathbf{r}_k \sim \mathrm{N}(\mathbf{0}, \mathbf{R}_k)$, then the linear measurement model is given by

$$\mathbf{y}_k = \mathbf{H}\mathbf{x}_k(\boldsymbol{\theta}) + \mathbf{r}_k \tag{6}$$

$\mathbf{H}$ is the measurement model matrix while $\mathbf{R}_k \in \mathbb{R}^{m \times m}$ is the covariance matrix of the zero mean Gaussian observation noise. Here, $n$ refers to the total number of time steps discretizing the time interval $[0, T]$.

Equations of the form of Eq. (5) are usually solved using *one-step* methods (Hughes 1987). Assuming the state vector $\mathbf{x}_k(\boldsymbol{\theta}) = \mathbf{m}_k(\boldsymbol{\theta})$ where $\mathbf{m}_k = (\mathbf{u}_k, \dot{\mathbf{u}}_k, \ddot{\mathbf{u}}_k)^{\mathrm{T}}$, the application of such *one-step* methods to Eq. (5) result in a single step time discretized recursive equation, for $k \in \{1, \dots, n\}$, of the form

$$\mathbf{m}_k = \mathbf{L}(\boldsymbol{\theta})\mathbf{m}_{k-1} + \mathbf{F}_k(\boldsymbol{\theta}) \tag{7}$$

The amplification matrix $\mathbf{L}(\boldsymbol{\theta})$ contains contributions from $\mathbf{M}(\boldsymbol{\theta})$, $\mathbf{C}(\boldsymbol{\theta})$ and $\mathbf{K}(\boldsymbol{\theta})$ while $\mathbf{F}_k(\boldsymbol{\theta})$ contains contributions from the external force.

## 3.  Posterior Probability Density and HMC

Parameter estimation is carried out through an approximation of the posterior probability distribution $p(\boldsymbol{\theta}|\mathbf{y}_{1:n})$ in a Bayesian framework. Following Bayes rule we can obtain

$$p(\boldsymbol{\theta}|\mathbf{y}_{1:n}) \propto p(\mathbf{y}_{1:n}|\boldsymbol{\theta})p(\boldsymbol{\theta}) \tag{8}$$

where $\mathbf{y}_{1:n}$ are the discrete observations and the proportionality sign implies the presence of a normalization constant which is not required in any MCMC algorithm. Based on the observation model in Eq. (6) and using $\mathbf{x}_k(\boldsymbol{\theta}) = \mathbf{m}_k(\boldsymbol{\theta})$, the likelihood function can be formed as

$$p(\mathbf{y}_{1:n}|\boldsymbol{\theta}) = \prod_{k=1}^{n} \mathrm{N}(\mathbf{y}_k|\mathbf{H}\mathbf{m}_k(\boldsymbol{\theta}), \mathbf{R}_k) \tag{9}$$

which when combined with a prior $p(\boldsymbol{\theta}) = \mathrm{N}(\boldsymbol{\theta}|\mathbf{0}, \boldsymbol{\Sigma_\theta})$, where $\boldsymbol{\Sigma_\theta}$ is the prior covariance matrix, completely defines the posterior.

Hamiltonian Monte Carlo (Duane et al. 1987; Neal 2011) is an MCMC algorithm that samples a probability distribution defined over the parameter space ($\boldsymbol{\theta} \in \mathbb{R}^K$) augmented with momentum variables ($\mathbf{p} \in \mathbb{R}^K$). The joint probability distribution is defined as

$$p(\boldsymbol{\theta}, \mathbf{p}) = p(\mathbf{p})p(\boldsymbol{\theta}|\mathbf{y}_{1:n}) \tag{10}$$

where, the probability distribution is usually defined as $p(\mathbf{p}) = \mathrm{N}(\mathbf{p}|\mathbf{0}, \mathcal{M})$. $\mathcal{M}$ is called as the mass matrix and has the main role of rotating and scaling the target parameter space to ensure efficient transitions. A term called the Hamiltonian ($H \in \mathbb{R}$) is then defined over this augmented space by simply taking the negative log of Eq. (10).

$$H(\boldsymbol{\theta}, \mathbf{p}) = -\log p(\boldsymbol{\theta}, \mathbf{p}) = -\log p(\mathbf{p}) + \varphi(\boldsymbol{\theta}) \tag{11}$$

The second component in Eq. (11), also called the potential energy ($\varphi \in \mathbb{R}$) is written as $\varphi(\boldsymbol{\theta}) = -\log p(\boldsymbol{\theta}|\mathbf{y}_{1:n})$.

HMC first involves a stochastic step where the new momentum variables are sampled as $\mathbf{p} \sim p(\mathbf{p})$. This is followed by a deterministic step that involves the solving of Hamilton's equations given by

$$\frac{d\boldsymbol{\theta}}{dt} = \frac{\partial H}{\partial \mathbf{p}} = \boldsymbol{\mathcal{M}}^{-1}\mathbf{p} \tag{12}$$

$$\frac{d\mathbf{p}}{dt} = -\frac{\partial H}{\partial \boldsymbol{\theta}} = -\frac{\partial \varphi(\boldsymbol{\theta})}{\partial \boldsymbol{\theta}} \tag{13}$$

Except for a few cases, these equations need to be solved numerically. The most popular numerical integrator for such a system in an MCMC setting is the Leapfrog method due to its properties of reversibility and volume preservation. Starting from $(\boldsymbol{\theta}, \mathbf{p})$ leapfrog integration is carried out for $L$ steps, with a step-size of $\varepsilon$, through the equations

$$\mathbf{p}\left(t + \frac{\varepsilon}{2}\right) = \mathbf{p}(t) - \frac{\varepsilon}{2}\frac{\partial \varphi(\boldsymbol{\theta}(t))}{\partial \boldsymbol{\theta}} \tag{14}$$

$$\boldsymbol{\theta}(t + \varepsilon) = \boldsymbol{\theta}(t) + \varepsilon \boldsymbol{\mathcal{M}}^{-1}\mathbf{p}\left(t + \frac{\varepsilon}{2}\right) \tag{15}$$

$$\mathbf{p}(t + \varepsilon) = \mathbf{p}\left(t + \frac{\varepsilon}{2}\right) - \frac{\varepsilon}{2}\frac{\partial \varphi(\boldsymbol{\theta}(t + \varepsilon))}{\partial \boldsymbol{\theta}} \tag{16}$$

This produces a new point $(\boldsymbol{\theta}^*, \mathbf{p}^*)$. The final step in HMC is the usual Metropolis accept-reject step, where the acceptance probability is given by

$$A(\boldsymbol{\theta}, \mathbf{p}; \boldsymbol{\theta}^*, \mathbf{p}^*) = \min(1, \exp\{-H(\boldsymbol{\theta}^*, \mathbf{p}^*) + H(\boldsymbol{\theta}, \mathbf{p})\}) \tag{17}$$

The critical question now is to determine how to update the parameters while maintaining acceptable mesh quality and how to calculate the gradient $\frac{\partial \varphi(\boldsymbol{\theta})}{\partial \boldsymbol{\theta}}$ in Eq. (13). Both these questions are addressed in the following section.

## 4.  Parameter Update

A simple mesh moving method and derivatives motivated by shape derivatives (commonly used in shape optimization) are used to carry out the parameter update.

### 4.1  Mesh moving method
The update of parameters in the domain through normal elastic deformation is likely to lead to large deformations and distortions of the mesh. A simple approach employed in this paper, to prevent such large distortions, is to use the classical moving mesh techniques (Stein et al. 2003; Tezduyar et al. 1992) popular in the computational fluid structure interaction literature. The simple idea is to introduce varying degrees of stiffness based on the element sizes, through the introduction of the mesh dependent element Young's modulus $E_e^m$, defined as

$$E_e^m = E_e \left(\frac{J^0}{J_e}\right)^\chi \tag{18}$$

$E_e$ is the usual Young's Modulus of element $e$ and $J_e$ is the determinant of the Jacobian associated with the transformation from physical to element (local) coordinates. $J^0$ is an arbitrary scaling parameter that makes the equation dimensionally consistent and $\chi$ is a positive number that provides varying degrees of stiffness to the corresponding elements. In the case that $\chi = 1$, the transformation Eq. (18) leads to a case where the Jacobian $J_e$ can just be dropped from the elemental stiffness matrix. The effect of such a transformation is that smaller elements become "stiffer" and deform rigidly (minimizing distortion) as compared to larger elements. The idea is then to place such rigid small elements near the cavity where most of the large deformations occur, while larger elements can be placed near the boundaries.

### 4.2  Evaluation of $\frac{\partial \varphi(\boldsymbol{\theta})}{\partial \boldsymbol{\theta}}$
Assume an updated parameterization $\boldsymbol{\theta}$ that produces the nodal coordinate update $\mathbf{Z}^0 \rightarrow \mathbf{Z}$, through the moving mesh technique described in Section 4. Then the updated node coordinates can be expressed as

$$\mathbf{Z}(\boldsymbol{\theta}) = \mathbf{Z}^0 + \mathbf{u}^m(\boldsymbol{\theta}) \tag{19}$$

where $\mathbf{u}^m \in \mathbb{R}^d$ represents the displacement during the moving mesh stage. Similar to Section 2, let $\mathbf{u}^m = (u_1^m, \dots, \mathbf{u}_c^m, \dots, u_d^m)$, where $\mathbf{u}_c^m = (u_{c1}^m, \cdots, u_{cd}^m)$ is the displacement of nodes at the cavity boundary. The displacement $\mathbf{u}^m$ arises from the elastic deformation produced in the domain due to the update of the nodes $\mathbf{Z}_c^0 \rightarrow \mathbf{Z}_c(\boldsymbol{\theta})$ such that $\mathbf{u}_c^m(\mathbf{Z}_c(\boldsymbol{\theta}) - \mathbf{Z}_c^0)$. It is straight forward to form explicit expressions for the cavity nodal displacements $\mathbf{u}_c^m(\boldsymbol{\theta})$ for simple cavity shapes such as the square shape considered in this paper.

The derivatives of the potential energy involve derivatives of the state vector $\frac{\partial \mathbf{m}_k}{\partial \boldsymbol{\theta}}$. Assuming no material damping in the domain, this derivative ultimately implies the calculation of $\frac{\partial \mathbf{M}(\boldsymbol{\theta})}{\partial \boldsymbol{\theta}}$ and $\frac{\partial \mathbf{K}(\boldsymbol{\theta})}{\partial \boldsymbol{\theta}}$. These derivatives are similar to those encountered in shape optimization (Haslinger and Makinen 2003). For element $e$, the derivatives of the elemental stiffness $\mathbf{K}_e$ and mass matrices $\mathbf{M}_e$ defined over the elemental domain $\Omega_e$ are given as

$$\frac{\partial \mathbf{K}_e(\boldsymbol{\theta})}{\partial \boldsymbol{\theta}} = \int_{\Omega_e} \left( \frac{\partial \mathbf{B}^{\mathrm{T}}}{\partial \boldsymbol{\theta}} \mathbf{D} \mathbf{B} J_e + \mathbf{B}^{\mathrm{T}} \mathbf{D} \frac{\partial \mathbf{B}}{\partial \boldsymbol{\theta}} J_e + \mathbf{B}^{\mathrm{T}} \mathbf{D} \mathbf{B} \frac{\partial J_e}{\partial \boldsymbol{\theta}} \right) t \rho \mathrm{d}\Omega_e \tag{20}$$

$$\frac{\partial \mathbf{M}_e(\boldsymbol{\theta})}{\partial \boldsymbol{\theta}} = \int_{\Omega_e} \mathbf{N}^{\mathrm{T}} \mathbf{N} \frac{\partial J_e}{\partial \boldsymbol{\theta}} t \rho \mathrm{d}\Omega_e \tag{21}$$

Following Haslinger and Makinen (Haslinger and Mäkinen 2003) expressions can be obtained for $\frac{\partial \mathbf{B}}{\partial \boldsymbol{\theta}} \left( \frac{\partial \mathbf{Z}}{\partial \boldsymbol{\theta}} \right)$ and $\frac{\partial J_e}{\partial \boldsymbol{\theta}} \left( \frac{\partial \mathbf{Z}}{\partial \boldsymbol{\theta}} \right)$ such that both are functions of $\frac{\partial \mathbf{Z}}{\partial \boldsymbol{\theta}}$. The derivatives of the updated node coordinates $\frac{\partial \mathbf{Z}}{\partial \boldsymbol{\theta}}$ are obtained from a simple differentiation of Eq. (19), given by

$$\frac{\partial \mathbf{Z}}{\partial \boldsymbol{\theta}} = \frac{\partial \mathbf{u}^m}{\partial \boldsymbol{\theta}} \tag{22}$$

This completes the definition of all components required for the computation of the gradient of potential energy.

### 4.3    Adaptive HMC and parameter constraints

The HMC algorithm is carried out for sampling $J$ samples, with $L$ leapfrog steps per sample. The inverse analysis procedure at the end of $L$ such leapfrog steps is the usual metropolis acceptance steps, where the acceptance probability $A$ is compared with a uniform number drawn from $\mathcal{U}(0,1)$. An adaptive version of HMC is used where $\varepsilon$ is set adaptively with diminishing adaptation in a similar manner to Robbins Monro (Robbins and Monro 1951). The adaptation used here is a variant of the Dual Averaging Scheme (Nesterov 2009), proposed by Hoffman and Gelman (Hoffman and Gelman 2011) for HMC.

An additional part of the HMC algorithm used in this study is the imposition of constraints on the parameters. Following the parameter update, a check is made on whether each component of the parameter lies within the respective lower ($lb$) or upper bounds ($ub$). If the condition is violated, the corresponding component of the momentum is flipped (Neal 2011) and the usual leapfrog steps resume. This alleviates the requirement of transformation of constrained parameters to an unbounded space and the calculation of the Jacobian involved with this transformation.

### 5.    Numerical Implementation and Results

The HMC framework proposed above is used to identify the position of a square cavity parameterized by $\boldsymbol{\theta} = [\theta_1, \theta_2, \theta_3]^{\mathrm{T}} = [z_1^{centre}, z_2^{centre}, l]^{\mathrm{T}} = [5, 5, 2]^{\mathrm{T}}$ as shown in Fig. 1(a). The elastic modulus of the domain is 25 MPa, density ($\rho$) is 2000 Kg/m$^3$ and Poisson's ratio 0.25. The mesh is generated in such a manner that more refined elements are placed near the cavity (Fig. 1(b)) while coarser elements are placed near the boundaries. The left and right boundaries are permitted to move only in the $z_2$ direction while Lysmer-Kuhlemeyer absorbing boundary condition was applied to the left, right and bottom boundaries. Observations, which comprise of velocities only, are recorded at all the time steps at the markers shown in Fig. 1(a). The domain is considered to be large enough and the observation points are placed in sufficiently far enough from any feasible position of the cavity. Synthetic data were generated using the true position of the cavity and an example of the synthetic waveform generated in the $z_2$ direction contaminated with Gaussian noise (mean=0 m/s, standard deviation = 10$^{-4}$ m/s), observed at a point on the top surface (marked green in Fig. 1(a)) is shown in Fig. 1(c). Even though no material damping is considered, the decrease in amplitude of velocity is due to the absorption of elastic waves at the absorbing boundaries. Numerical integration is performed using the Newmark-$\beta$ scheme with $\gamma = 0.5$ and $\beta = 0.25$ in the forward problem.

A total of 2000 samples were generated using HMC starting from an initial point $\boldsymbol{\theta}^1 = [2, 2.5, 1]^{\mathrm{T}}$ shown on the left in Fig. 2. The number of leapfrog steps per HMC sample is sampled from a Gaussian i.e. $L \sim \mathrm{N}(25,3)$. $J_\varepsilon = 500$ steps were considered for adaptation, which was ultimately found to be sufficient as the Markov chains converged well within this limit. These 500 initial steps are considered as *burn-in* and discarded in all post processing steps. The initial step size was chosen as $\varepsilon^1 = 0.001$ and standard parameter values (Hoffman and Gelman 2011) of Dual Averaging were used in this analysis. Both, the mass matrix $\mathcal{M}$ and $\boldsymbol{\Sigma}_{\boldsymbol{\theta}}$ were chosen as the identity matrix $\mathbf{I}_3$. The lower bound and upper bound vectors for the parameters are $\boldsymbol{\theta}^{lb} = [1, 1, 0.5]^{\mathrm{T}}$ and $\boldsymbol{\theta}^{ub} = [9, 9, 7]^{\mathrm{T}}$ respectively.

(a)                                                                                          (b)
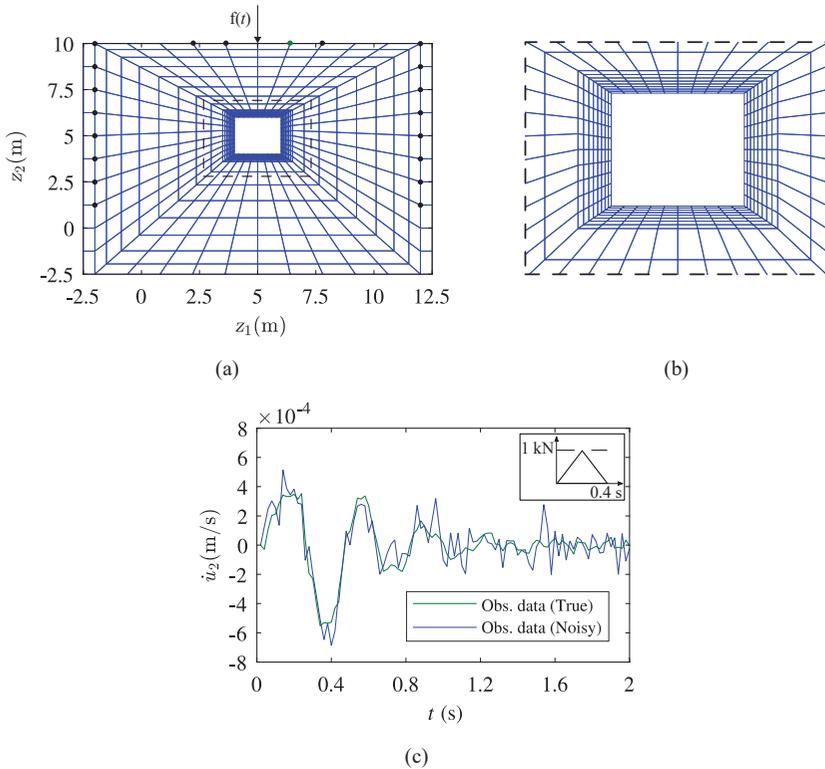


(c)

**Figure 1.** (a) Schematic showing position of true cavity along with mesh and observation points. (b) Zoomed version of the refined mesh near the cavity. (c) $z_2$ component of true and noisy observed velocity at (6.4, 10), see left figure, in response to a triangular load (inset) of 1 kN applied for 0.4 s.
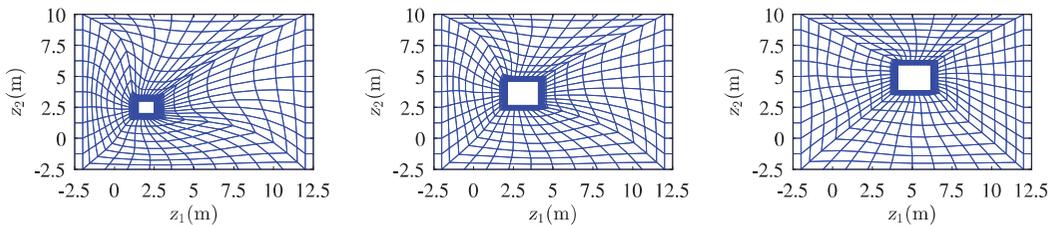


**Figure 2.** Mesh at different stages of HMC: (left) step 1, (middle) step 50 and (right) step 500.
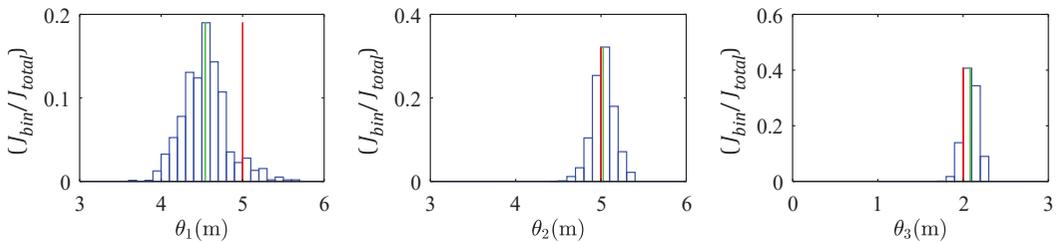


**Figure 3.** Normalized bin counts for $\boldsymbol{\theta}$. $J_{bin}$ and $J_{total}$ represent the number of samples in a bin and the total number of samples respectively. Red and green lines represent the true and HMC mean parameter values respectively.

Starting from $\boldsymbol{\theta}^1$ the mesh gradually advances towards the solution. Fig. 2 shows the mesh at different stages ($j$) of HMC. It can be seen that the small elements near the cavity deform rigidly and prevent large distortions. The normalized bin counts for the components of $\boldsymbol{\theta}$ along with the true and HMC mean parameter values are plotted in Fig. 3 using only the samples after *burn-in*. The estimated mean from HMC is $\boldsymbol{\theta} = [4.54, 5.03, 2.09]^{\mathrm{T}}$. Fig. 3 also shows the confidence in the estimated parameters. It can clearly be seen that the estimated values of $\theta_2$ and $\theta_3$ are close to the true values while $\theta_1$ is slightly biased. This is clearly reflected in the variance of the parameters. While the normalized bin count $\theta_2$ and $\theta_3$ is sufficiently high and concentrated near the true solution, the corresponding values for $\theta_1$ are smaller and more dispersed.

## 6. Conclusions

A framework in which a square cavity (parameterized by the coordinates of its center and its side length) can be estimated in an HMC framework is presented. The key components of this framework are the Moving Mesh method and the shape derivatives employed to evaluate the gradient. Inverse analysis on artificially generated noisy data validates the proposed framework. The advantage of this HMC based framework is the ability of the parameters to vary continuously over the confined parameter space making the estimated solution independent of mesh discretization. The explicit consideration of the shape produces another advantage in terms of the ability to accurately resolve the cavity boundaries which is a major drawback in many inverse analysis methods.

**References**

Duane, S., Kennedy, A.D., Pendleton, B.J., and Roweth, D. (1987). Hybrid Monte Carlo. *Physics Letters B*, 195(2), 216–222.

Guzina, B.B., and Bonnet, M. (2004). Topological derivative for the inverse scattering of elastic waves. *Quarterly Journal of Mechanics and Applied Mathematics*, 57(2), 161-179.

Haslinger, J. and Mäkinen, R.A. (2003). *Introduction to Shape Optimization- Theory, Approximation, and Computation*, SIAM, Philadelphia.

Hoffman, M.D. and Gelman, A. (2011). The No-U-Turn sampler: Adaptively setting path lengths in Hamiltonian Monte Carlo. *arXiv*, 15, 1351–1381.

Hughes, T.J.R. (1987). *The Finite Element Method: Linear Static and Dynamic Finite Element Analysis*, *Inc.*, Prentice-Hall, New Jersey.

Lysmer, J. and Kuhlemeyer, R.L. (1969). Finite dynamic model for infinite media. *Journal of the Engineering Mechanics Division*, 95, 859–877.

Metropolis, N., Rosenbluth, A.W., Rosenbluth, M.N., Teller, A.H., and Teller, E. (1953). Equation of state calculations by fast computing machines. *The Journal of Chemical Physics*, 21(6), 1087–1092.

Neal, R.M. (2011). *Handbook of Markov Chain Monte Carlo*, chapter 5: MCMC using Hamiltonian dynamics, CRC Press.

Nesterov, Y. (2009). Primal-dual subgradient methods for convex problems. *Mathematical Programming*, 120(1), 221–259.

Nguyen, L.T. and Nestorović, T. (2016). Unscented hybrid simulated annealing for fast inversion of tunnel seismic waves. *Computer Methods in Applied Mechanics and Engineering*, 301, 281-299.

Robbins, H. and Monro, S. (1951). A stochastic approximation method. *The Annals of Mathematical Statistics*, 22(3), 400–407.

Stein, K., Tezduyar, T., and Benney, R. (2003). Mesh moving techniques for fluid-structure interactions with large displacements. *Journal of Applied Mechanics*, 70, 58–63.

Tezduyar, T.E., Behr, M., Mittal, S., and Johnson, A.A. (1992). Computation of unsteady incompressible flows with the stabilized finite element methods: space-time formulations, iterative strategies and massively parallel implementations. *Asme Pressure Vessels Piping Div Publ PVP*, 246, 7–24.